Nickel Octaethylporphyrin Ruffling Dynamics from Resonance Raman Spectroscopy

Roman S. Czernuszewicz, Xiao-Yuan Li, and Thomas G. Spiro*

Contribution from the Department of Chemistry, Princeton University, Princeton, New Jersey 08544. *Received November 14, 1988*

Abstract: Resonance Raman spectra for nickel octaethylporphyrin (NiOEP) in solution are compared with triclinic and tetragonal crystalline forms containing flat and ruffled porphyrin. The appearance in solution of several bands that are activated only in the crystals containing ruffled porphyrin and that have been assigned to porphyrin out-of-plane modes provides clear evidence for a ruffled structure in solution. The in-plane porphyrin skeletal modes and their isotope shifts are catalogued for the triclinic and tetragonal crystals. The similarities in isotope shift pattern and relative RR intensities show that the normal-mode compositions are not significantly altered by ruffling, even though there are appreciable frequency shifts. The solution frequencies are intermediate between those of the triclinic and tetragonal crystals, indicating that the degree of ruffling is diminished in solution relative to the ruffled NiOEP crystals. The structure-sensitive ν_{10} band has been examined in detail. It is much broader in solution than in either of the crystals. The band profile covers the frequency range from the flat (1663 cm^{-1}) to the ruffled (1642 cm^{-1}) structures, peaking at $\sim$1653 cm^{-1}; a range of solution structures is inferred. The previous treatment by Asher and Murtaugh of the temperature dependence of ν_{10} in terms of anharmonic coupling with a low-frequency mode is explicitly related to the B_{1u} pyrrole swiveling mode, γ_{12} = 610 cm^{-1} in the tetragonal crystals, which is involved in the ruffling distortion. This mode is absent in solution and is suggested to soften when the crystal packing constraints are removed. The resulting flattening of the γ_{12} potential provides a physical mechanism for the breadth of ν_{10} and the temperature dependence of its central frequency. NiOEP ruffling strengthens the NiN bonds at the expense of the porphyrin π conjugation, low-spin Ni^{2+} being slightly smaller than the standard porphyrin cavity size. The dynamics of porphyrin ruffling and the associated behavior of ν_{10} are not typical of metalloporphyrins in general; it is shown that the ν_{10} band of $[(ImH)_2Fe^{III}OEP]^+$ (ImH = imidazole) is much narrower than that of NiOEP. Consequently application of the NiOEP ν_{10} temperature dependence to pulsed laser RR spectra of heme proteins, as in the case of the picosecond transient RR study of hemoglobin-CO photolysis by Petrich et al., probably overestimates the heating contribution. The reported 11-cm^{-1} downshift of ν_4 measured 0.9 ps after a 0.2-ps photolysis pulse is probably too large to be attributed to heating alone and may reflect contributions from partially relaxed electronic states and from undissociated CO.

In preceding articles[1] the normal modes of nickel octaethylporphyrin (NiOEP) have been analyzed, taking advantage of the favorable chemical and electronic properties of the molecule and also of its polymorphism in the solid state. NiOEP crystallizes in isomeric forms with different relative orientations of the ethyl substituents and also with different conformations of the porphyrin ring itself. Triclinic crystals[2a,b] contain flat porphyrin rings, but in tetragonal crystals[2c] a propellor twist of the pyrrole rings ruffles the skeleton (see Figure 1). This ruffling is attributable to the low-spin Ni^{2+} ion being slightly smaller than the standard porphyrin cavity size.[3] The propellor distortion permits the NiN(pyrrole) bonds to shorten, by 0.02-0.03 Å relative to the flat structures. This strengthening of the NiN bonds is at the expense of the porphyrin π conjugation, which is optimized when the macrocycle is flat. The polymorphism indicates that the planar and ruffled structures are nearly equal in energy, the form isolated depending on crystallization conditions.[2] The question naturally arises where the balance of these forces lies in NiOEP solutions, when the molecules are unconstrained by packing forces, and what the consequences are for the solution structure.

In this study we investigate this question by comparing solution resonance Raman (RR) spectra with those of flat and ruffled structures in crystals. We are able to conclude that NiOEP is definitely ruffled in solution, although not by as much as in the tetragonal crystals. Independent evidence for nonplanar solution structures has been presented by Shelnutt and co-workers[20]. The breadth of the solution RR bands, particularly of the highest frequency in-plane porphyrin skeletal mode ν_{10}, demonstrates a range of coexisting structures. We infer that the opposing forces favoring flat vs ruffled structures are manifested in a flattening of the potential for a B_{1u} normal mode, γ_{12}, whose eigenvector involves a propellor twist displacement of the pyrrole rings. This mode has been assigned[1b] at 612 cm^{-1} in the low-temperature (12 K) crystal RR spectra of the ruffled form (610 cm^{-1} in room-temperature spectra), and its disappearance in the solution spectrum is suggested to result from mode softening.

These findings throw light on the previous observation by Asher and Murtaugh[4] of a strong ν_{10} temperature dependence for NiOEP in solution or in the vapor phase. The decreasing frequency with increasing temperature can be explained by an increase in the ruffled population due to increasing thermal excitation of the flattened B_{1u} propellor coordinate. This special dynamical aspect of the NiOEP RR spectrum makes it a poor predictor of the temperature dependence of metalloporphyrin vibrational frequencies in general, as advocated by Asher and Murtaugh.[4] They were concerned about the possibility that frequency shifts in transient heme protein photoproducts that had been attributed to unrelaxed states of the protein might instead be due to laser heating of the porphyrin. Subsequently Petrich et al.[5] measured an 11-cm^{-1} downshift in the ν_4 mode of the CO-hemoglobin photoproduct, 0.9 ps after photolysis. Using Asher and Murtaugh's analysis of the NiOEP ν_{10} temperature dependence, they attributed the shift to a 218 K temperature rise due to laser heating. Because ν_{10} of NiOEP is especially temperature-sensitive, the heating effect on the photoproduct RR frequency was probably overestimated. We discuss the possibility of alternative explanations involving unrelaxed electronic states and delayed dissociation of CO.

* Author to whom correspondence should be addressed.

(1) (a) Paper 2 of this series: Li, X.-Y.; Czernuszewicz, R. S.; Kincaid, J. A.; Stein, P.; Spiro, T. G. *J. Phys. Chem.*, in press. (b) Paper 3 of this series, Li, X.-Y.; Czernuszewicz, R. S.; Kincaid, J. R.; Spiro, T. G. *J. Am. Chem. Soc.*, preceding article in this issue.

(2) (a) Cullen, D. L.; Meyer, E. F., Jr. *J. Am. Chem. Soc.* **1974**, *96*, 2095-2102. (b) Brennan, T. D.; Scheidt, W. R.; Shelnutt, J. A. *J. Am. Chem. Soc.* **1988**, *110*, 3919-3924. (c) Meyer, E. F., Jr. *Acta Crystallogr.* **1972**, *B28*, 2162-2167.

(3) Hoard, J. L. In *Porphyrins and Metalloporphyrins*; Smith, K. M., Ed.; Elsevier: Amsterdam, 1975; Chapter 8.

(4) Asher, S. A.; Murtaugh, J. *J. Am. Chem. Soc.* **1983**, *105*, 7244-7251.

(5) Petrich, J. W.; Martin, J. L.; Houde, D.; Poyart, C.; Orszag, A. *Biochemistry* **1987**, *26*, 7914-7923.

0002-7863/89/1511-7024$01.50/0

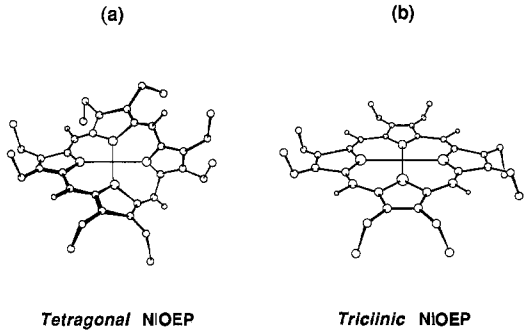

Figure 1. Structural diagram of NiOEP showing ruffled (a) and flat (b) porphyrin rings in the known crystal structures of the tetragonal[2c] and the two triclinic forms.[2a,b] The triclinic A form is shown; the B form has altered ethyl orientations.[1a]

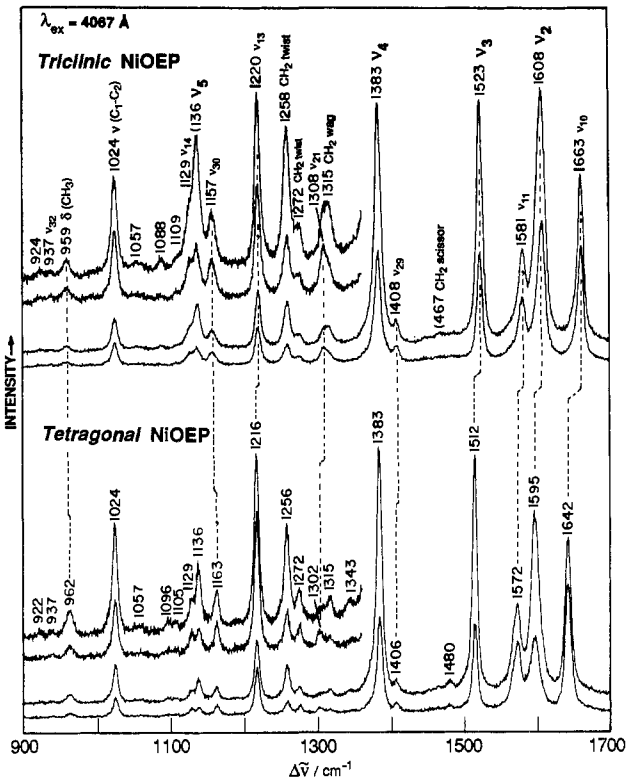

Figure 2. The 4067-Å excited RR spectra of triclinic (top) and tetragonal (bottom) crystals of NiOEP in the 900–1700-cm^{-1} region at room temperature (∥ and ⊥ are parallel and perpendicular components, respectively). Conditions: backscattering from spinning KCl pellets,[19] 150-mW laser power, 3-cm^{-1} slit widths; one scan, 1-s integration time at 0.5-cm^{-1} increments. The dashed lines correlate structure sensitive bands.

Experimental Section

NiOEP and its isotopomers were prepared according to the methods described in ref 1a. The preparation of tetragonal and triclinic crystalline samples[2] is described in the preceding article.[1b] $(ImH)_2Fe^{III}(OEP)ClO_4$ was prepared as described in ref 6. Resonance Raman spectra were collected in backscattering geometry from a spinning NMR tube (solution spectra) or from KCl pellets (solid-state spectra), which were either rotated at room temperature or kept at 12 K on the cold finger of a Model CSA-202E closed-cycle liquid He refrigerator (Air Products, Allentown, PA).[19]

Excitation radiation for RR measurements was provided by a Spectra Physics 171 Kr^+ laser. The scattered light was dispersed by a Spex 1401 double monochromator and detected by a cooled RCA 31034A photomultiplier tube using an ORTEC 9315 photon-counting system, under the control of a MINC II (DEC) minicomputer. Other experimental conditions are given in the figure captions.

(6) (a) Ogoshi, H.; Watanabe, E.; Yoshida, Z.; Kincaid, J.; Nakamoto, K. *J. Am. Chem. Soc.* **1973**, *95*, 2845–2849. (b) Mitchell, M.; Li, X.-Y.; Kincaid, J. R.; Spiro, T. G. *J. Phys. Chem.* **1987**, *91*, 4690–4696.

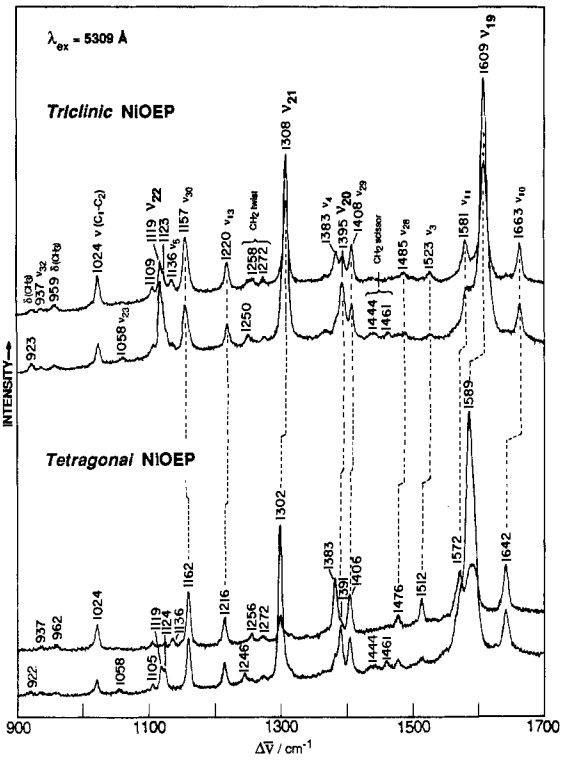

Figure 3. As for Figure 2, but with 5309-Å excitation.

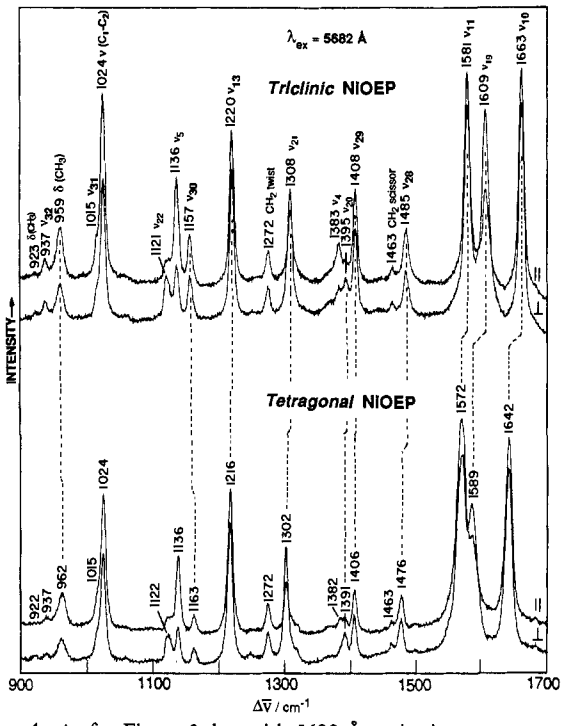

Figure 4. As for Figure 3, but with 5682-Å excitation.

Results and Discussion

In-Plane Skeletal Mode Frequencies of Planar Versus Ruffled NiOEP. Spaulding et al.[7] noted appreciable frequency shifts between corresponding RR bands of crystalline NiOEP in triclinic and tetragonal forms. In Figures 2–4, we examine in detail the differences in the region above 900 cm^{-1}, using three excitation wavelengths, 406.7, 530.9, and 568.2 nm, which bring out respectively the A_{1g}, the A_{2g}, and the B_{1g} and B_{2g} modes of the porphyrin. The intensity patterns are quite similar for the two

(7) Spaulding, L. D.; Chang, C. C.; Yu, N.-T.; Felton, R. H. *J. Am. Chem. Soc.* **1975**, *97*, 2517–2525.

Table I. RR Frequencies and ^{15}N Isotope Shifts (cm^{-1}) for NiOEP in CS_2 Solution and in Crystalline Samples[a]

	tetragonal crystals[c]			triclinic crystals[d]				
soln[b] na	na ($\Delta^{15}N$)	d_4 ($\Delta^{15}N$)	d_{16}	na ($\Delta^{15}N$)	d_4 ($\Delta^{15}N$)	d_{16}	ρ	assgnt[e]
1655	1642 (0)	1631 (0)	1642	1663 (0)	1651 (0)	1662	dp	ν_{10}, B_{1g}
1602	1595 (1)	1595 (1)	1589	1608 (1)	1606 (1)	1601	po	ν_2, A_{1g}
1603	1589 (1)	1569 (1)	1586	1609 (1)	1586 (1)	1608	ap	ν_{19}, A_{2g}
1577	1572 (0)	1571 (0)	1565	1581 (0)	1580 (0)	1574	dp	ν_{11}, B_{1g}
1520	1512 (1)	1506 (1)	1512	1523 (1)	1515 (1)	1522	p	ν_3, A_{1g}
1483	1476 (3)	1471 (2)	1373	1485 (3)	1479 (2)	1482	dp	ν_{28}, B_{2g}
1464	1467 (0)	1466 (0)	1146	1467 (0)	1466 (0)	1148	p	CH_2 scissor, A_1
1463	1463 (0)	1462 (0)	1169	1463 (0)	1462 (0)	1169	dp	CH_2 scissor, B_1
1462	1461 (0)	1462 (0)	1148	1461 (0)	1461 (0)	1148	ap	CH_2 scissor, A_2
1441	1444 (0)	1444 (0)	1139	1444 (0)	1444 (0)	1138	ap	CH_2 scissor, E_u
1407	1406 (1)	1406 (1)	1405	1408 (1)	1405 (1)	1404	dp	ν_{29}, B_{2g}
1393	1391 (0)	1391 (0)	1387	1395 (0)	1393 (0)	1389	ap	ν_{20}, A_{2g}
1383	1383 (7)	1381 (7)	1379	1383 (7)	1382 (7)	1380	p	ν_4, A_{1g}
1368	1368 (0)	1368 (0)	1363	1368 (0)	1367 (0)	1363	ap	?
1330[f]		1328 (5)			1328 (5)		dp	ν_{12}, B_{1g}
1316	1315 (0)	1315 (0)	839	1315 (0)	1316 (0)	840	p	CH_2 wag, A_1
1312	1310 (0)	1310 (0)		1310 (0)	1310 (0)		dp	CH_2 wag, B_1
		1306 (0)			1308 (0)		ap	CH_2 wag, A_2
1307	1302 (4)	882 (5)	1296	1308 (4)	888 (5)	1303	ap	ν_{21}, A_{2g}
1276	1272 (1)		831	1272 (1)		832	dp	CH_2 twist, B_1
1258	1256 (1)	1256[g]	1258	1258 (1)	1259 (1)[g]		p	CH_2 twist, A_1
1252	1246 (0)	1256 (0)		1250 (0)	1259 (0)		ap	CH_2 twist, A_2
1220	1216 (2)	1182 (2)	1240	1220 (2)	1184 (2)	1246	dp	ν_{13}, B_{1g}
1159	1163 (12)	1161 (11)	1095	1157 (12)	1157 (12)	1096	dp	ν_{30}, B_{2g}
1138	1136 (7)	1137 (7)	1068	1136 (7)	1137 (8)	1068	p	ν_5, A_{1g}
1131	1129 (14)	949 (10)	1075	1129 (14)	948 (11)	1074	dp	ν_{14}, B_{1g}
1121	1119 (15)	1203 (14)	1109	1119 (14)	1198 (13)	1109	ap	ν_{22}, A_{2g}
1126	1124 (1)	1126 (2)	1176	1123 (5)	1126 (1)	1177	ap	?
1109	1105 (0)	1107 (0)	1106	1109 (0)	1108 (0)	1107	dp	?
1058	1058 (0)	1057 (0)	993	1058 (0)	1058 (0)	993	ap	ν_{23}, A_{2g}
1024[f]	1024 (4)[f]	1030 (0)	1206	1024 (4)[f]	1030 (0)	1206	dp	$\nu(C_1C_2)$, B_1
1024[f]	1024 (4)[f]	1024 (3)	1189	1024 (4)[f]	1024 (3)	1189	p	$\nu(C_1C_2)$, A_1
1015	1015 (9)	1003 (10)	988	1015 (10)	1003 (10)	989	dp	ν_{31}, B_{2g}
960[f]	962 (2)[f]			959 (3)[f]			dp	$\rho(CH_3)$, B_1
960[f]	962 (2)[f]	963 (3)		959 (3)[f]	960 (4)		p	$\rho(CH_3)$, A_1
938	937 (0)	935 (0)	974	937 (0)	934 (0)	973	dp	ν_{32}, B_{2g}
922	922 (0)	938 (0)		923 (0)	938 (0)		ap	$\rho(CH_3)$, A_2

[a] Values observed at room temperature RR spectra; na = natural abundance, d_4 and d_{16} = ^2H substituted analogues at meso carbons and methylene positions, respectively; $\Delta^{15}N$ = shifts upon ^{15}N pyrrole substitution in na and d_4 species; not available for d_{16} isotopomer. [b] CS_2 solution data taken from ref 1a. [c] Pure crystal form. [d] ~50/50 mixture of A and B forms. [e] See ref 1a for band assignments. [f] Seen only in the meso-d_4 isotopmers. [g] Broad bands; the 1256-cm^{-1} band of tetragonal crystals is resolved into a double (1253/1257 cm^{-1}e in the d_4, ^{15}N double isotopomer spectra. [i] Overlapping bands.

crystal forms, making band correspondences obvious. Moreover, the isotope shifts, ^{15}N, meso-d_4, and methylene-d_{16} (not shown), are essentially the same and are given in Table I. It is clear that the normal-mode compositions do not differ between the forms, despite noticeable frequency shifts. Samples of triclinic crystallites are mixtures of A and B forms, which have different orientations of the ethyl groups.[2b] Brennan et al. found small A–B frequency differences for the modes above 1000 cm^{-1}, up to 4 cm^{-1}, and attributed these to intermolecular stacking interactions in the B form[2b] (although the ethyl orientations might also contribute to these differences[1a]). The A–B differences are too small to be resolved in the spectra of the mixtures, and the frequencies listed in Table I should be considered average values for the A and B forms.

All of the skeletal frequencies above 1400 cm^{-1} are lower in the ruffled than in the flat form. (The $\delta(CH_2)$ ethyl modes[1a] are unaltered.) This effect is reminiscent of the frequency lowerings for the same modes associated with an increase in the porphyrin core size.[8] The trend seems paradoxical since ruffling actually contracts the core, to accommodate the short Ni–N(pyrrole) bonds.[2] It might be argued that ruffling produces an effect similar to core expansion because the interruption of the π conjugation by ruffling should weaken the methine bridge bonds, as core expansion does.[9] Inspection of the NiOEP crystal structures, however, fails to show significant weakening of the methine bridge bonds. The average C_aC_m distance is essentially the same, 1.372 Å, in the ruffled structure[2c] as in the flat structures A[2a] (1.371 Å) or B[2b] (1.365 Å).

Table II. Correlation of Flat–Ruffled Frequency Differences (cm^{-1}) with Core Size Sensitivities for NiOEP[a]

mode	triclinic	tetragonal	Δ,[b] cm^{-1}	K,[c] cm^{-1}/Å
ν_{10} (B_{1g})	1663	1642	21	564.9
ν_{28} (B_{2g})	1485	1476	9	494.4
ν_{19} (A_{2g})	1609	1589	20	450.0
ν_3 (A_{1g})	1523	1512	11	423.7
ν_{11} (B_{1g})	1581	1572	9	353.1
ν_2 (A_{1g})	1609	1595	14	329.3
ν_4 (A_{1g})	1383	1385	0	136.7

[a] Frequencies from room-temperature spectra. [b] Triclinic–tetragonal. [c] Slope of the frequency/core size dependence from ref 9.

Table II shows that the correlation between the flat–ruffled frequency differences and the core size sensitivities (slopes of the frequency vs core size plots)[7] is actually far from exact. Although the core size slopes cover a continuous range from 330 to 565 cm^{-1}/Å, the flat–ruffled differences cluster around values near 0, 10 cm^{-1} or 20 cm^{-1}. It is of interest that the four modes involving C_aC_m stretching primarily, ν_3, ν_{28}, ν_{19}, and ν_{10}, show 10- or 20-cm^{-1} differences depending on whether they involve the in-phase combination of adjacent bridge bond stretches, ν_3 (A_{1g}) and ν_{28} (B_{2g}), or the out-of-phase combination, ν_{19} (A_{2g}) and ν_{10} (B_{1g}). This dependence on the phasing suggests that the frequency shifts may be associated with kinematic effects of the ring distortion, which

(8) Parthasarathi, N.; Hansen, C.; Yamaguchi, S.; Spiro, T. G. *J. Am. Chem. Soc.* **1987**, *109*, 3865–3871.
(9) Choi, S.; Spiro, T. G.; Langry, K. C.; Smith, K. M.; Budd, L. D.; LaMar, G. N. *J. Am. Chem. Soc.* **1982**, *104*, 4345–4351.

Table III. Comparison of In-Plane Mode Frequencies (cm^{-1}) in RR Spectra of NiOEP in Solution and Crystalline Samples[a]

solution	tetragonal	triclinic A	triclinic B	ρ	assgn[b]
804	804	803	804	p	ν_6, A_{1g}
781	779	780	782	dp	CH_2 rock, B_1
769	765	768	770	p	CH_2 rock, A_1
751	750	749	752	dp	ν_{15}, B_{1g}
	746 (sh)	738	741	dp	ν_{16}, B_{1g}
674	674	674	674	p	ν_7, A_{1g}
597		591	591	ap	ν_{24}, A_{2g}
551		551	551	ap	ν_{25}, A_{2g}
493	484	494	494	dp	ν_{33}, B_{2g}
343/360[c]	350 (348)[d]	350 (343)	357 (354)	p	ν_8, A_{1g}
	328	327/332[e]	326/330[e]	p	ν_{51}, E_u
307	320 (sh)	309	316	dp	ν_{17}, B_{1g}
272/263[c]	290 (282)	289 (278)	283 (278)	p	ν_9, A_{1g}
	263			dp	ν_{52}, E_u
	212			p	ν_{53}, E_u
201	202	196	204	dp	ν_{34}, B_{2g}
170	179	172	172	dp	ν_{18}, B_{1g}
143	152	143	143	dp	ν_{35}, B_{2g}

[a] Observed values in CH_2Br_2 solution at room temperature and KCl pellets (crystalline NiOEP) at 12 K.[1b] [b] See ref 1a for mode assignments. [c] Pairs of frequencies attributed to ethyl orientational isomers.[1a] [d] Selected room-temperature frequencies shown in parentheses; the ν_8 and ν_9 modes show unusually large temperature variations, which may be related to ethyl conformation effects.[1a] [e] Weak bands; tentative assignment.[1a]

affect the in- and out-of-phase combinations differently, rather than with valence force constant changes. On the other hand force constant changes may account for the ~10-cm^{-1} downshifts of ν_2 and ν_{11}, which involve $C_\beta C_\beta$ stretching primarily, since the $C_\beta C_\beta$ bond is noticeably longer in the ruffled structure, 1.362 Å,[2c] than in the flat structures, 1.346[2c] and 1.332 Å[2b] for A and B forms.

In the spectral region between 900 and 1400 cm^{-1} the triclinic–tetragonal frequency differences are 6 cm^{-1} for ν_{21} (1308 cm^{-1}), −6 cm^{-1} for ν_{30} (1157 cm^{-1}), and 3 cm^{-1} or less for the remaining bands.

Table III compares in-plane skeletal mode frequencies below 900 cm^{-1} in tetragonal crystals, in the A and B forms in triclinic crystals, and in CS_2 solution. The solid-state data were obtained at low temperature (12 K) to permit resolution of closely spaced bands and deconvolution of the A and B spectra, which show appreciable differences in the low-frequency region.[1b] These differences have been attributed to the ethyl orientational isomerism and reflect substantial involvement of the ethyl coordinates in the low-frequency modes. This effect can be seen in solution as well through the doubling of two of the low-frequency modes, ν_8 and ν_9.[1b] The frequency differences between the triclinic and the tetragonal crystals may reflect both the ethyl orientational isomerism and the influence of the porphyrin ruffling.

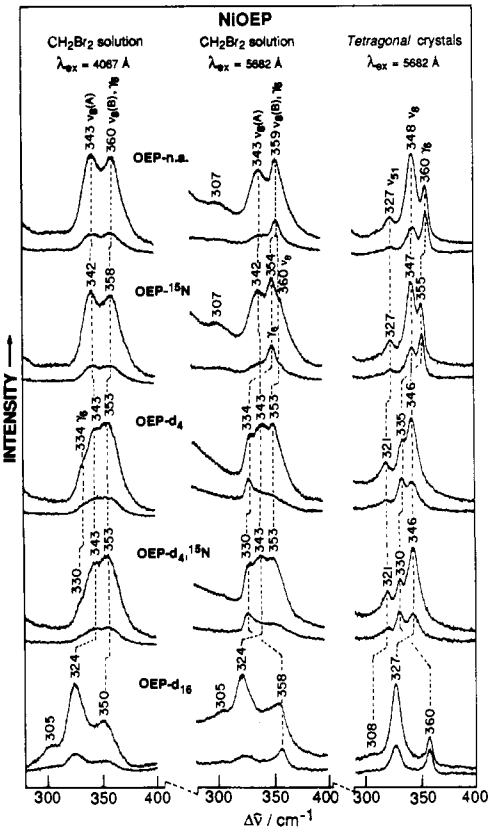

Figure 5. Solution (in CH_2Br_2, left and middle panels) and tetragonal crystal (in KCl, right panel) RR spectra of NiOEP and its isotopically labeled samples in the 300–400-cm^{-1} region with the indicated excitations. Conditions: backscattering from spinning NMR tube (solution spectra) or from spinning KCl pellet (solid-state spectra); 150-mW laser power; 3-cm^{-1} slit widths; two scans, 1-s integration time at 0.2-cm^{-1} increments.

Table I lists solution frequencies for the high-frequency modes showing the largest triclinic–tetragonal differences. In every case the solution frequency is at an intermediate value between those of the two crystalline samples. These results suggest that NiOEP adopts an intermediate structure in solution.

Table IV. Comparison of Out-of-Plane Mode Frequencies (cm^{-1}) in RR Spectra of NiOEP in CH_2Br_2 Solution and Tetragonal Crystals[a]

solution			tetragonal crystals				
na (Δ^{15}N)	d_4 (Δ^{15}N,n)	d_{16}	na (Δ^{15}N)	d_4 (Δ^{15}N)	d_{16}	ρ	assign[b]
853 (0)		842[c]				p	$\gamma_{10}(B_{1u})$, $\gamma(C_mH)$
847 (0)		832[c]	843 (0)		839	dp	$\gamma_4(A_{2u})$, $\gamma(C_mH)$
847 (0)			841 (0)[d]			ap	$\gamma_{19}(E_g)$, $\gamma(C_mH)$
			749 (3)[e]	749 (0)	736	dp	$\gamma_1(A_{1u})$, pyr $fold_{asym}$
739 (6)	762 (3)[c]	737	738 (6)	760 (2)[c]	730	dp	$\gamma_5(A_{2u})$, pyr $fold_{sym}$
735 (3)[f]			732 (0)			p	γ_{11} (B_{1u}), pyr $fold_{asym}$
715 (9)		716	720 (10)		719	+	$2\gamma_6$
712 (7)[g]	702 (4)	700	703 (4)	701 (4)	701	p	γ_{15} (B_{2u}), pyr $fold_{sym}$
			610 (0)	652 (0)	603	p	γ_{12} (B_{1u}), pyr swivel
549 (2)	530 (1)	530	548 (2)	528 (1)	529	p	δ_5 (E_g), $\delta(C_\beta C_1 C_2)_{asym}$
			523 (0)	523 (0)	500	dp	δ_2 (A_{2u}), $\delta(C_\beta C_1 C_2)_{sym}$
469 (0)	468 (0)	463	474 (1)	474 (1)	470	p	δ_4 (B_{2u}), $\delta(C_\beta C_1 C_2)_{sym}$
433 (0)	428 (0)	419	442 (0)	440 (0)	424	dp	δ_1 (A_{1u}), $\delta(C_\beta C_1 C_2)_{asym}$
359 (5)[h]	334 (4)	358	360 (5)	335 (5)	360	dp	γ_6 (A_{2u}), pyr tilt
			282 (0)[i]	277 (0)	277	dp	γ_7 (A_{2u}), $\gamma(C_\alpha C_m)$
			249 (3)	249 (3)	246	p	γ_{23} (E_g), pyr tilt
224 (2)	224 (2)	222	223 (3)[d]	223 (3)[d]	221[d]	p	γ_{24} (E_g), $\gamma(C_\alpha C_m)$
144 (0)[j]	141 (0)[j]	144[j]	124 (0)	124 (0)	124	p	γ_{17} (B_{2u}), $\gamma(C_\beta C_1)_{sym}$

[a] See footnote *a* in Table I. [b] See ref 1b for band assignments. [c] Overlapping bands (see ref 1a). [d] These frequencies from triclinic crystal RR spectra. [e] Overlaps with ν_{15} (see ref 1b). [f] Seen with 4067-Å excitation; its small ^{15}N sensitivity results from the overlapping with γ_5 (see text). [g] Seen with 5309-Å excitation; this band overlaps with $2\gamma_6$ as judged from its larger than expected ^{15}N shift (7 vs 4 cm^{-1}). [h] Overlaps with ν_8. [i] Overlaps with ν_9, but it is resolved in low-temperature spectra (see ref 1b). [j] Overlaps with ν_{35}.

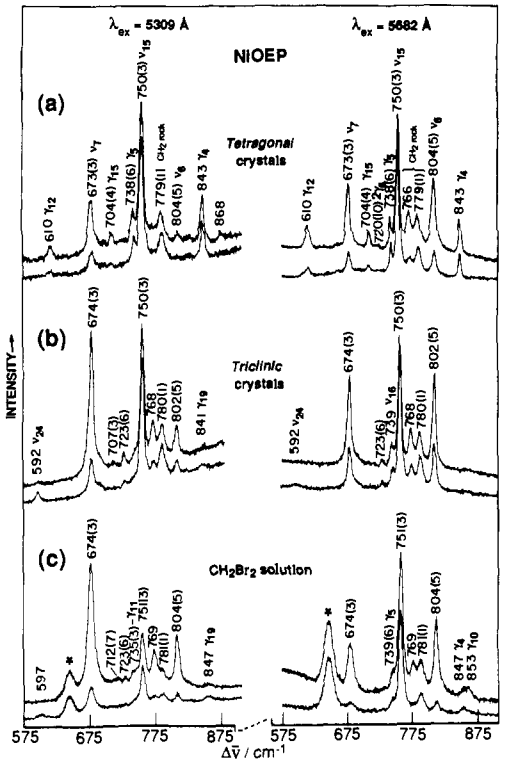

Figure 6. The 575–875-cm^{-1} region RR spectra of NiOEP with 5309-Å (left panel) and 5682-Å (right panel) excitations: (a) tetragonal crystals; (b) triclinic crystals; (c) CH_2Br_2 solution (solvent bands are indicated by asterisks). Conditions: as in Figure 5, but for these data the spectrometer was advanced in 0.5-cm^{-1} increments. Frequency shifts upon pyrrole ^{15}N substitution are shown in parentheses.

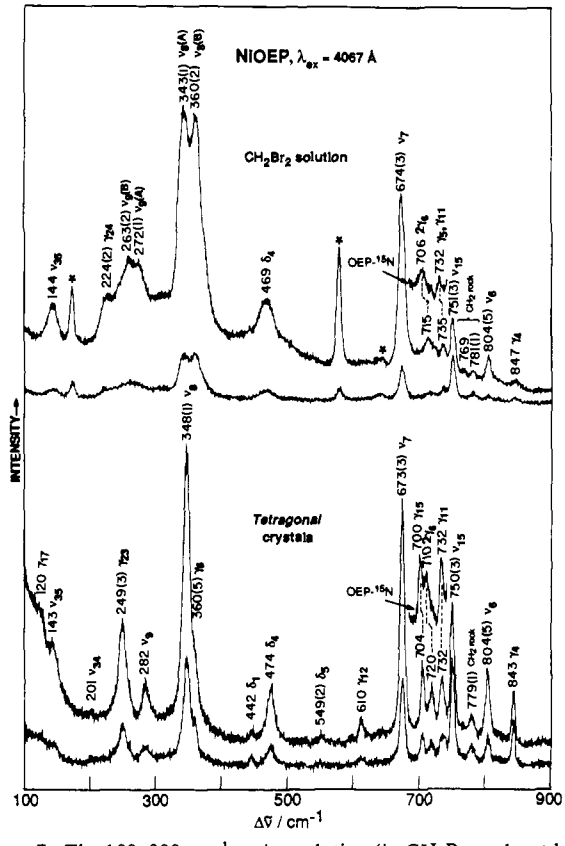

Figure 7. The 100–900-cm^{-1} region solution (in CH_2Br_2, solvent bands are indicated by asterisks) and tetragonal crystal (KCl pellet) NiOEP RR spectra with 4067-Å excitation. Insets show NiOEP ^{15}N spectra (parallel component only) identifying the 715- (solution) and 720-cm^{-1} (solid) bands with the first overtone of the out-of-plane pyrrole tilting γ_6 mode. ^{15}N isotope shifts for the remaining bands are given in parentheses. The pairs ν_8(A), ν_8(B) and ν_9(A), ν_9(B) in solution spectra are believed to arise from molecules with different ethyl orientations.[1a] Conditions are as in Figure 6.

Out-of-Plane Mode Activation in Solution. We now present unambiguous evidence from the activation of out-of-plane (oop) modes, listed in Table IV, that NiOEP is ruffled in solution. (See the preceding paper[1b] for the oop mode numbering and assignments.) Figure 5 compares 568.2-nm excited RR spectra in the 350-cm^{-1} region for NiOEP in solution and in tetragonal crystals (middle and right panels).

The latter show two prominent bands, γ_6 at 360 cm^{-1} and ν_8 at 348 cm^{-1}, with different polarizations and isotope shifts; a weaker 327-cm^{-1} band is assigned to an E_u mode, ν_{51}, activated by the porphyrin ruffling.[1a] The ν_8 breathing mode involves a concerted motion of the pyrrole rings along the NiN bonds, mixed with symmetric ethyl bending.[1a] It gives rise to a polarized band that is sensitive to methylene deuteration (d_{16}) but nearly insensitive to ^{15}N substitution or methine deuteration (d_4). The γ_6 pyrrole tilting oop mode gives rise to a depolarized band that is d_{16}-insensitive but shifts down strongly in the ^{15}N (5 cm^{-1}) and d_4 (26 cm^{-1}) isotopomers. The differing polarizations make it easy to track the two bands as shown by the vertical lines in Figure 5.

In solution (middle panel) there is clearly a depolarized band at 359 cm^{-1}, which has the isotope shift pattern characteristic of γ_6. The 359-cm^{-1} band envelope also contains one of the two ν_8 bands seen in solution, the other being at 343 cm^{-1}. As in triclinic crystals that contain A and B forms, each giving rise to a separate ν_8 band, the solution bands are believed to reflect ethyl orientational isomerism.[1a] When γ_6 is shifted out of the way upon d_4 substitution, the two ν_8 bands are clearly revealed. They differ in their sensitivity to d_4 and d_{16} substitution, reflecting differences in the extent of ethyl involvement.[1a] When 4067-Å excitation is used to generate the solution spectra (left panel), the γ_6 band is much weaker in relation to the ν_8 bands, but it can still be detected in the d_4 and d_4, ^{15}N spectra, in which it is shifted out of the ν_8 envelope.

The γ_6 mode is activated in tetragonal crystals because the porphyrin ruffling lowers the symmetry to S_4 and the A_{2u} modes correlate with the B representation. They are consequently subject to resonance enhancement by vibronic coupling or Jahn–Teller activity. 5682-Å excitation, in resonance with the Q band, produces maximal enhancement of B-symmetry modes that are active in Q/B mixing.[1a] In spectra of triclinic crystals there is no trace of γ_6 (see Figure 5 of the preceding paper[1b]). Thus its activation is clearly associated with porphyrin ruffling. The fact that γ_6 is activated in solution therefore establishes that the solution structure is ruffled.

Further evidence for ruffled structure in solution is provided by the RR bands in the 850-cm^{-1} region seen in Figure 6, where out-of-plane wagging modes of the methine H atoms are expected. The tetragonal crystals show a prominent depolarized band at 843 cm^{-1}, assigned to the γ_4 (A_{2u}) mode.[1b] The triclinic crystals show only a very weak band at 841 cm^{-1}, assigned to γ_{19} (E_g) (E_g oop modes are allowed for planar NiOEP, and candidate bands have been identified in the low-temperature spectra of the triclinic crystals[1b]). The solution spectrum shows a depolarized band at ~847 cm^{-1}, as well as a polarized companion at ~853 cm^{-1}, both of which are shifted out of the region upon meso-d_4 substitution. The former is assigned to γ_4 as in the tetragonal crystals, while the latter is suggested to be γ_{10} (A in S_4 symmetry). Other out-of-plane modes which are detectable in the solution Q-band-excited spectra (Figure 6) are the pyrrole folding modes γ_{15} (712 cm^{-1}) and γ_5 (739 cm^{-1}; Table IV). γ_5 can be distinguished from the nearly coincident in-plane ν_{16} mode by its strong (6 cm^{-1}) ^{15}N downshift (not shown). Conspiciously missing from the solution spectra is the pyrrole swiveling mode, γ_{12} at 610 cm^{-1} (vide infra).

Figure 7 compares solution and tetragonal crystal RR spectra in resonance with the B band (4067-Å excitation). Activation of γ_6 is again readily detectable, especially in the tetragonal

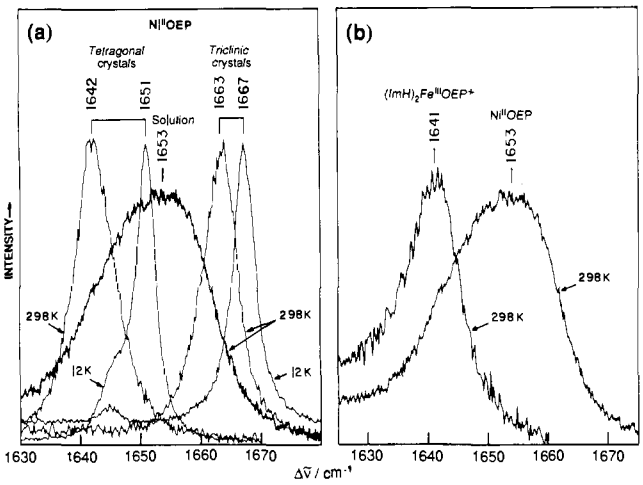

Figure 8. (a) ν_{10} vibrational mode profiles in resonance Raman spectra of NiOEP in CH_2Br_2 solution at room temperature (298 K) and in tetragonal and triclinic crystals at room (298 K) and low (12 K) temperatures. (b) Comparison of the ν_{10} RR band profiles of $(ImH)_2Fe^{III}OEP^+$ and NiOEP in CH_2Br_2 solution at room temperature. Conditions: backscattering from spinning NMR tube (solution spectra) or from KCl pellet attached to a cold finger of a CSA-202E closed-cycle liquid He refrigerator;[19] 5682-Å excitation; 200-mW laser power; 1-cm^{-1} slit width; 3 scans, 1-s integration time at 0.2-cm^{-1} increments.

crystals when ν_8 interference is minimized, and the $2\gamma_6$ overtone can also be seen at 720 cm^{-1}, clearly identifiable by its 10-cm^{-1} ^{15}N downshift (see insets), twice the γ_6 shifts. The overtone is detectable in solution as well as tetragonal crystals. Another pyrrole tilting mode, γ_{23} (E_g) at 249 cm^{-1} is also activated in the tetragonal crystals. In solution a broad complex feature is seen in this region, which is believed to contain two ν_9 bands, again resulting from ethyl isomerism;[1a] γ_{23} may also contribute to this envelope. The appearance in solution of a 224-cm^{-1} shoulder with 2-cm^{-1} ^{15}N sensitivity suggests that still another oop mode, γ_{24} (E_g),[1b] is activated. In the ~800-cm^{-1} region one again sees the $\gamma(C_mH)$ mode γ_4, giving depolarized 843- and 847-cm^{-1} bands in crystals and solution, respectively (presumably Jahn–Teller activated), and the pyrrole folding mode γ_{11}, giving a polarized band at 732 cm^{-1}. γ_{11} is distinguishable from the overlapping γ_5 (B) mode by its polarization as well as its ^{15}N insensitivity (vs 6-cm^{-1} ^{15}N shift for γ_5). Both γ_{11} and γ_5 contribute to the 735-cm^{-1} solution band, which shows an apparent 3-cm^{-1} ^{15}N shift. The 704-cm^{-1} γ_{15} band appears in the crystal spectrum but not in the solution spectrum, even though it is activated in solution with 5309-Å excitation (Figure 6).

An interesting feature in Figure 7 is the prominent very broad band at 469 cm^{-1} in solution. This replaces the relatively strong 474-cm^{-1} and weak 445-cm^{-1} crystal bands, which are assigned to ethyl bending modes, δ_4 and δ_1. We infer that these modes are spread over a range of frequencies by ethyl orientational isomerism in solution.

The picture that emerges from this analysis of the oop modes is of a solution structure that is significantly nonplanar. The similarity of the enhancement pattern to that of NiOEP in tetragonal crystals implies that the porphyrin is similarly ruffled in solution, although the degree of the ruffling may not be as large, in view of the intermediacy of the solution in-plane mode frequencies between those of tetragonal and triclinic crystals. The range of ethyl conformations in solution, which is reflected in the breadth of the 469-cm^{-1} ethyl bending mode, may also account for some of the differences with respect to the crystal spectra including the apparent activation of additional out-of-plane modes, γ_{10} and γ_{24}.

Structural Variation: The ν_{10} Band Shape. Not only are the solution RR bands of the high-frequency NiOEP in-plane modes intermediate in frequency between those of the flat (triclinic) and ruffled (tetragonal) crystal forms, but the bands are significantly broadened in solution. The behavior of the highest frequency band, ν_{10}, is shown in Figure 8.

At room temperature triclinic and tetragonal crystals show bands of 7-cm^{-1} width (fwhm) which peak at 1663 and 1642 cm^{-1}. When the samples are cooled to 12 K, the peaks narrow substantially (4-cm^{-1} fwhm) and shift up in frequency. (An unidentified 1645-cm^{-1} shoulder is also revealed for tetragonal crystals at 12 K.) For triclinic crystals the ν_{10} upshift is 4 cm^{-1}, within the 1–5-cm^{-1} range of upshifts seen for most other porphyrin bands when samples are cooled to 12 K. The 9-cm^{-1} ν_{10} upshift for tetragonal crystals is well outside this range. Since ν_{10} is higher for flat than ruffled NiOEP, the extra upshift for the ruffled form suggests a tendency for the ring to flatten at low temperature.[10] This would be consistent with the spontaneous conversion of flat to ruffled NiOEP at elevated temperature,[8] demonstrating that the flat form is more stable at low temperature. The ruffled structure does not fully reconvert to the flat structure, presumably due to the constraints of crystal packing; even at 12 K the ν_{10} frequency is substantially lower for the tetragonal than the triclinic crystals. Nevertheless, one can envision a low-temperature diminution in the out-of-plane displacement of the pyrrole rings within the ruffled structure.

The most significant finding from the ν_{10} profiles is the large width, 24-cm^{-1} fwhm, of the NiOEP solution band. The band is much broader than other solution bands, which are typically 10–15 cm^{-1} wide. Likewise other porphyrins do not have unusually broad ν_{10} bands; Figure 8 illustrates this point with the ν_{10} band of $[(ImH)_2Fe^{III}OEP]^+$ (ImH = imidazole) at 1641 cm^{-1}, which has a 10-cm^{-1} width. Although the ν_{10} peak frequency for NiOEP in solution has an intermediate value, 1653 cm^{-1}, the inflection points of the band coincide with the ν_{10} peaks for triclinic and tetragonal crystals and the wings merge with those of the two solid forms at room temperature (Figure 8). We conclude that there must be a range of structures in solution, with different degrees of ruffling.

The number of structures is uncertain. With a little broadening it would be possible to fit the solution band profile with three peaks, one each at the flat and ruffled positions and one in between. It is also consistent with the data, however, that the solution structures cover a continuous range between flat and fully ruffled.

Asher and Murtaugh[4] studied the temperature dependence of the NiOEP ν_{10} band and observed that its frequency decreases with elevated temperature for NiOEP dissolved in silicone oil and attains a frequency of 1640 cm^{-1} in the gas phase at 650 K. This frequency is fully as low as that observed for solid ruffled NiOEP at room temperature. Thus the solution (and gas phase) data are consistent with a shift in the distribution of structures toward the ruffled form at elevated temperatures, consistent with the spontaneous conversion of flat to ruffled NiOEP in the solid state upon heating.

Softening of the Pyrrole Twisting Mode: Structural Dynamics and Anharmonic Coupling. Asher and Murtaugh[4] interpreted the temperature dependence of the ν_{10} frequency as evidence for anharmonic coupling of ν_{10} to a low-frequency mode. Treatment of the data according to this model gave an estimate of 528 ± 150 cm^{-1} for the frequency of the coupling mode. They considered the coupling mode to be one that leads to expansion of the porphyrin core, on the basis of the known core size sensitivity of ν_{10} in metalloporphyrins.[8] The mode that is best described as a porphyrin core expansion mode is ν_8, at ~350 cm^{-1}, which involves the four pyrrole rings moving away from the Ni atom in a concerted fashion (see Figure 13 of ref 1a for the eigenvector). While this frequency is within the large uncertainty range of the coupling mode frequency estimate by Asher and Murtaugh, ν_8 seems unlikely to be the coupling mode because there is no reason to think that it should uniquely influence the ν_{10} frequency of NiOEP. All metalloporphyrins would have their cores expanded by ν_8, which should then couple to all of the core size marker bands in proportion to their sensitivities to core expansion. The $[(ImH)_2Fe^{III}OEP]^+$ spectrum (Figure 8) illustrates the point that a general pattern of ν_{10} broadening is not seen.

The coupling mechanism should instead be sought in the special

(10) Scheuermann, W.; Nakamoto, K. *J. Mol. Struct.* **1978**, *48*, 285–288.

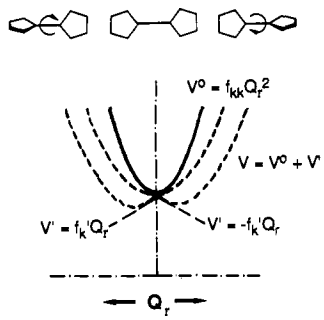

Figure 9. Conceptual diagram of the softening of a mode Q_r which allows Ni–N(pyrrole) bond contraction by swiveling the pyrrole rings and ruffling the porphyrin. The Ni–N bond extension in the flat structure ($Q_r = 0$) produces a force, $\pm f_k'$, which lowers the potential by a linear (for small displacements) term, V'. This flattens the otherwise quadratic potential, V^0, or, for large enough f_k', can lead to a double-minimum potential.

structural dynamics of NiOEP itself, which involves the ruffling of the porphyrin ring in response to the small size of the low-spin Ni^{2+} ion. Various normal modes can contribute to the motion which leads to the ruffled structure, but for the sake of simplicity we consider a single ruffling mode, Q_r, which is diagrammed in Figure 9. In a strain-free flat metalloporphyrin Q_r would be harmonic with a minimum at the flattened position ($Q_r = 0$). The extension of the Ni–N bond beyond its optimum distance, however, introduces a force that favors a displacement along Q_r, leading to Ni–N bond contraction. This force can be thought of as adding a linear term to the quadratic potential, producing an anharmonic potential. (For large displacements the added term would be nonlinear; indeed in the absence of the forces favoring a planar structure a new harmonic potential would result that is displaced along Q_r to a position corresponding to the optimum Ni–N bond length). The effect of the anharmonicity is to flatten the Q_r potential, or, if the contracting force is large enough, to produce a double-minimum potential. The effect of the flattening is to reduce the frequency of the Q_r mode and allow a range of ruffled structures whose distribution should be temperature sensitive as the Q_r vibrational levels become thermally excited. This provides a natural explanation for the breadth of the ν_{10} band and the shift in its peak frequency with increasing temperature. In crystals the packing forces determine the most stable structure and effectively quench the Q_r anharmonicity, thereby sharpening the ν_{10} band. Structural variation is still possible, however, as indicated by the large ν_{10} downshift on cooling the tetragonal crystals, suggesting a flatter structure at low temperature.

In considering the nature of Q_r, we call attention to the B_{1u} mode γ_{12}, identified in the tetragonal crystals at 612 cm^{-1}.[1b] As noted above, the 612-cm^{-1} band is absent in the solution spectra, even though other oop bands are seen clearly. Its absence is consistent with significant mode softening (anharmonicity), which would shift the band to lower frequency and broaden it, perhaps out of recognition. The γ_{12} eigenvector is shown in Figure 10. It involves swiveling of the pyrrole rings, the motion that is required to shorten the Ni–N bonds. The 612-cm^{-1} frequency is in the range estimated by Asher and Murtaugh[4] for the mode(s) that induces the temperature sensitivity of ν_{10} via anharmonic coupling. The softening of γ_{12} provides an effective mechanism for the coupling.

Comparison of the γ_{12} eigenvector with the static structure in tetragonal crystals (Figure 10) shows that the motion resembles the observed ruffling, but the match is not exact, since the C_m atom motions are counter to the observed structure. A better match is provided by another B_{1u} mode, γ_{14} (see Figure 10), which is unobserved but is calculated[1b] at 44 cm^{-1}. The much lower frequency of this mode makes it an easier distortion coordinate for trapping by crystal packing forces. Nevertheless, it is likely that in solution γ_{12} as well as γ_{14} provide effective pathways for Ni–N bond shortening and are both softened.

Raman Frequencies as Indicators of Heat Dissipation in Pulsed Laser Experiments: Hemoglobin Photolysis. Asher and Murtaugh[4] used the ν_{10} temperature dependence to estimate the

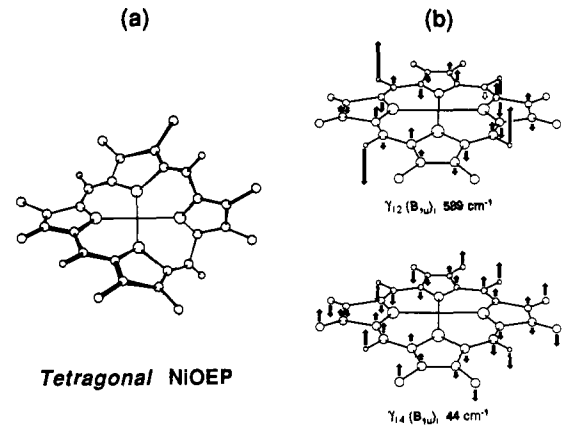

Figure 10. Eigenvectors of the B_{1u} modes, γ_{12} and γ_{14}, which can provide effective pathways for Ni–N bond shortening and porphyrin ruffling. These modes are suggested to soften in solution.

possible heating effects on RR spectra associated with the use of picosecond laser pulses, taking into account the finite thermal dissipation rate after photoexcitation. Following this suggestion Petrich et al.[5] interpreted their picosecond RR results on the CO adduct of hemoglobin (Hb) photolysis in terms of heat dissipation. They photodissociated HbCO and monitored the ν_4 RR band of the product with 0.2-ps laser pulses. Downshifts relative to equilibrium deoxy-Hb were observed, and they decreased with time: 11.0, 7.6, 2.2, and 3.0 cm^{-1}, respectively, at 0.9, 2, 9.4, and 30 ps (increasing again, to 6.2 cm^{-1} at 95 ps). The relaxation of the frequency shift is on the time scale expected for heat dissipation on the basis of molecular dynamics calculations on myoglobin by Henry et al.,[11] who found 50% of the cooling occurring in 1–4 ps and the remainder in 20–40 ps. Using the anharmonic coupling model and the parameters reported by Asher and Murtaugh for the NiOEP ν_{10} band, Petrich et al. calculated a 218 K temperature rise of the photolyzed HbCO at 0.9 ps. As demonstrated in the preceding section, however, the NiOEP ν_{10} dynamics is atypical of metalloporphyrin RR bands in general. A better callibration might be the temperature dependence of ν_4 in deoxy-Hb itself. According to spectra reported by Friedman and Rousseau[12] the frequency difference between deoxy-Hb at 300 K and frozen to 4.2 K is only 3 cm^{-1}. Thus the 11-cm^{-1} shift of the HbCO photoproduct at 0.9 ps seems too large to be attributed to a heating effect alone, and alternative explanations should be considered.

Since absorption of a photon by HbCO is to the porphyrin π–π^* level, the possibility arises that π–π^* states contribute to the evolving photoproduct. Population of the π–π^* states is expected to lower the frequency of ν_4 and other porphyrin skeletal modes, on the basis of RR spectral shifts seen for porphyrin radical anions,[13] and has been invoked to explain large downshifts of several RR bands when HbO_2 is photolyzed with intense 30-ps pulses.[14] For HbCO, however, electronic relaxation associated with photolysis seems to be very fast. According to the subpicosecond transient absorption results of Martin et al.,[15] the formation of a deoxy-Hb-like spectrum after HbCO excitation occurs with a 0.35-ps time constant. In a subsequent study Petrich et al.[16] found an additional intermediate with a 2.5-ps lifetime upon photolyzing HbO_2 and HbNO, but its yield for HbCO was low. Thus electronically excited heme seems an unlikely explanation

(11) Henry, E. R.; Levitt, M.; Eaton, W. A. *Proc. Natl. Acad. Sci. U.S.A.* **1985**, *82*, 2034–2038.
(12) Rousseau, D. L.; Friedman, J. M. In *Biological Applications of Raman Spectroscopy*; Spiro, T. G., Ed.; Wiley-Interscience: New York, 1989; Vol. III, pp 172–180.
(13) Gurinovich, G. P.; Gurinovich, I. F.; Ivanshin, N. V.; Sinyakov, G. N.; Shulga, A. M.; Terekov, S. N.; Filatov, I. V.; Dzilinski, K. *J. Mol. Struct.* **1988**, *172*, 317–343.
(14) Terner, J.; Voss, D. F.; Paddock, C.; Miles, R. B.; Spiro, T. G. *J. Phys. Chem.* **1982**, *86*, 859–861.
(15) Martin, J. L.; Migus, A.; Poyart, C.; Lecarpentier, Y.; Staastier, R.; Antonetti, A. *Proc. Natl. Acad. Sci. U.S.A.* **1983**, *80*, 173–177.
(16) Petrich, J. W.; Poyart, C.; Martin, J. L. *Biochemistry* **1988**, *27*, 4049–4060.

for the RR spectral shifts upon HbCO photolysis.

Very recently Rothberg et al.[17] have obtained picosecond infrared spectra on photolyzed HbCO that indicate a transient high-yield photoproduct with a 2-ps lifetime and a CO stretching frequency suggestive of a high-spin heme adduct. The persistence of such a complex for times longer than the electronic relaxation to the high-spin state has previously been considered[18] as an explanation for the heme core size expansion which is detected in RR transient spectra extending to 10 ns. This explanation was rejected for the longer time scale, but a 2-ps lifetime for a high-spin Fe–CO complex as suggested by the results of Rothberg et al. is not implausible. Although ν_4 is only weakly dependent on the porphyrin core size,[8] the proposed CO binding to the high-spin heme might contribute to the early ν_4 shift through polarization effects. Indeed it is possible that there are multiple contributions to the ν_4 shift on the ~2-ps time scale, from heating, from partially unrelaxed electronic states, and from undissociated CO. The heating effect itself needs to be evaluated in an experimental system which is more closely related to the HbCO photoproduct ν_4 band than is the ν_{10} band of NiOEP.

Conclusions

NiOEP is clearly ruffled in solution, as evidenced by activation of several of the out-of-plane modes seen in tetragonal crystals.

In-plane skeletal mode frequencies of NiOEP in solution are intermediate between tetragonal and triclinic crystal frequencies, suggesting an intermediate structure.

A large ν_{10} band width implies a range of structures in solution.

These observations, as well as the temperature dependence of the ν_{10} frequency, are suggested to result from anharmonic potentials, possibly double-welled, for the γ_{12} and γ_{14} pyrrole swiveling modes, which arise from the countervaling forces favoring planar versus ruffled NiOEP.

This special effect does not apply to metalloporphyrin bands in general, and the NiOEP ν_{10} temperature dependence is not a reliable guide to the magnitude of heating effects expected in pulsed laser experiments on heme proteins.

Acknowledgment. This work was supported by NIH Grant GM33576. We are deeply grateful to Dr. J. R. Kincaid, Marquette University, for providing us with samples of NiOEP isotopomers and to Drs. R. H. Austin and L. Rothberg for communicating results of their work prior to publication.

Registry No. NiOEP, 24803-99-4.

(17) Rothberg, L.; Jedju, T. M.; Austin, R. H., submitted for publication.
(18) Dasgupta, S.; Spiro, T. G. *Biochemistry* **1986**, *25*, 5941-5948.
(19) Czernuszewicz, R. S. *Appl. Spectrosc.* **1986**, *40*, 571-573.
(20) Alden, R. G.; Crawford, B. A.; Ondrias, M. R.; Shelnutt, J. A. *Proc. Int. Conf. Raman Spectrosc., XI*; Clark, R. J. H., Long, D. A., Eds.; Wiley: New York, 1988; p 541.

Characterization of the Electronic Structure of 4′,6-Diamidino-2-phenylindole

Mikael Kubista,* Björn Åkerman, and Bo Albinsson

Contribution from the Department of Physical Chemistry, Chalmers University of Technology, 412 96 Gothenburg, Sweden. *Received December 16, 1988*

Abstract: We characterize the electronic structure of 4′,6-diamidino-2-phenylindole (DAPI) in terms of electronic transition energies, transition moment directions, and oscillator strengths in the UV–vis region. The study is based on linear dichroism and fluorescence anisotropy measurements of DAPI dissolved in poly(vinyl alcohol) film, magnetic circular dichroism in aqueous solution, and circular dichroism on DAPI dissolved in *d*-tartrate and bound to DNA.

The cation 4′,6-diamidino-2-phenylindole (DAPI) binds to double-stranded DNA with a concomitant increase in fluorescence quantum yield.[1] This property has made DAPI very useful as a probe for DNA in gel electrophoresis,[2,3] in DNA protein interactions,[4-6] in cytochemical investigation,[7-12] and for staining of mammalian chromosomes.[13] The binding of DAPI to DNA is reversible, and the molecule binds in two spectroscopically distinct sites, both located in the grooves of DNA.[14-16] To correctly interpret the spectroscopic features of free DAPI and in complexes with DNA and proteins, it is necessary to characterize its spectroscopic properties. In this work we combine information from linear dichroism (LD), fluorescence polarization anisotropy (FPA), circular dichroism (CD), and magnetic circular dichroism (MCD) measurements to elucidate the electronic properties of DAPI in the UV–vis region.

Materials and Methods

Chemicals. All chemicals used were of analytical grade and aqueous solutions were prepared with deionized triply filtered water (Milipore). DAPI was purchased from Serva and used without purification. Poly(vinyl alcohol) (PVA) was obtained as powder from E. I. du Pont de

(1) Kapuscinski, J.; Szer, W. *Nucleic Acids Res.* **1979**, *6*, 3519-3534.
(2) Kapuscinski, J.; Yanagi, K. *Nucleic Acids Res.* **1979**, *6*, 3535-3542.
(3) Naimski, P.; Bierzynski, A.; Fikus, M. *Anal. Biochem.* **1980**, *54*, 385-394.
(4) Kai, J.; Fanning, T. G. *Eur. J. Biochem.* **1976**, *67*, 367-371.
(5) Stepien, E.; Filutowicz, M.; Fikus, M. *Acta Biochem. Pol.* **1979**, *26*, 29-38.
(6) Mazus, B.; Falchuk, K. H.; Vallee, B. L. *Biochemistry* **1986**, *25*, 2941-2945.
(7) Williamson, D. H.; Fennel, D. J. *Methods Cell Biol.* **1975**, *12*, 335-351.
(8) Schweizer, D. *Exp. Cell Res.* **1976**, *102*, 408-409.
(9) Langlois, R. G.; Carrano, A. V.; Stay, J. W.; van Dilla, M. A. *Chromosoma* **1980**, *77*, 229-251.
(10) Coleman, A. W.; Maguire, M. J.; Coleman, J. R. *J. Histochem. Cytochem.* **1981**, *29*, 959-968.
(11) Tijssen, J. P. F.; Beekes, H. W.; van Steveninck, J. *Biochem. Biophys. Acta* **1982**, *721*, 394-398.
(12) Lee, G. M.; Thornthwaite, J. T.; Rasch, E. M. *Anal. Biochem.* **1984**, *137*, 221-226.
(13) Lin, M. S.; Alfi, O. S.; Donnell, G. N. *Can. J. Genet. Cytol.* **1976**, *18*, 545-547.
(14) Manzini, G.; Barcellona, M. L.; Avitabile, M.; Quadrofoglio, F. *Nucleic Acids Res.* **1983**, *11*, 8861-8876.
(15) Kubista, M.; Åkerman, B.; Nordén, B. *Biochemistry* **1988**, *26*, 4545-4553.
(16) Kubista, M.; Åkerman, B.; Nordén, B. *J. Phys. Chem.* **1988**, *92*, 2352-2356.

0002-7863/89/1511-7031$01.50/0